FOM Institute AMOLF TUDelft

Contacting Single Core-Shell Nanowires for Photovoltaics

Internship report by	: C. Sfiligoj
Student number	: 4185765
Research group	: Nanoscale Solar cells
Group Leader and External Supervisor	: Dr. E. C. Garnett
Internal supervisor	: Dr. J. R. Gao
Period	: October 2013 - April 2014

Abstract

The performance of conventional planar solar cells is limited by a fundamental trade-off for which increasing the absorption of light by thickening the semiconductor layer in contrast increases the production costs and decreases the charge collection efficiency.
A controlled tailoring of the properties of nanostructures could potentially help to overcome this limit. Among the various geometries, nanowires (NWs) have proven to be particularly promising building blocks for photovoltaic (PV) applications.
In this project I focus on metal-semiconductor core-shell NWs. Theoretical studies have shown that this type of NWs have optical properties, not available in solid semiconductor NWs, that allow to maximize light absorption by using only few nanometers of material. In addition, the metal core can be used as metal electrode and thus in principle improve charge collection.
The purpose of my project is to experimentally investigate the photovoltaic properties of core-shell NWs by applying electrical contacts to them (one on the core and the other on the shell) using a fabrication process based on electron-beam lithography. To create a PV device, the additional challenge is to find the right metallization scheme such that photogenerated carriers can be efficiently separated and extracted.
For my experiments I used NWs dispersed in solution, with Cu_2O as semiconductor shell and Ag or Au as metal cores. The NWs transferred on a SiN_x/Si substrate with Au pads and markers, specifically designed for e-beam lithography. After defining an efficient and reliable route to fabricate the metallic contacts, I studied different metallization schemes.
Measurements on Au@Cu_2O NWs with Ti shell contacts and Au core contacts showed a strong rectifying behavior and an increase in photoconductivity under 1 sun illumination. However no photovoltaic effect has been detected, suggesting that diffusion length of photogenerated carriers is too short compared to the distance that the charges have to travel to reach the metal electrode without recombining.
By increasing the power of illumination to 200 μW using a 404 nm-laser beam focused in proximity of the shell contact a photocurrent of $\sim$400 pA has been measured.
These results encourage further research towards more efficient PV devices and possible methods can be immediately tested to improve the charge collection efficiency of the current Au@Cu_2O NWs.

Contents

Chapter 1

Introduction to Nanowire Solar Cells

1.1 Conventional Solar Cells and Future Prospects with Nanotechnology

In the search for renewable energies, solar cells are very promising and they can satisfy a good part of the growing electrical power demand [1,2]. However, the current costs of electricity generated by photovoltaic (PV) systems are still too high compared to fossil energy sources. In order to make the solar market more competitive it is necessary to achieve higher conversion efficiencies and reduce material costs.
So-called *first generation* solar cells are the dominant technology in the commercial production of solar cells, accounting for more than 86% of the PV market. Cells are typically made using a crystalline silicon wafer. However, one of the biggest limits is that silicon has a relatively low absorption coefficient throughout much of the visible and near-infrared parts of the electromagnetic spectrum; since most of the light coming from the sun is in this range, silicon-based solar cells must be thick in order to collect most of the incident photons.
Second generation solar cells are made thin in order to reduce material costs, but this in turn reduces light absorption [3].
Third generation solar cells are emerging technologies aimed to overcome the limits of previous solar cells. The latest and most interesting developments have been centered on the use of nanotechnology given the fundamental advantages that nanostructures have demonstrated compared to their bulk counterparts. These include supreme light absorption [4,5] and promoted charge separation and collection in high-impurity materials [6,7]. Among the various nanostructured architectures, nanowires (NWs) seem very promising for photovoltaics [8].
In the present work I focus on a specific type of NW geometry, with a metal core embedded in an ultrathin semiconducting shell.

1.2 Why are Metal-semiconductor Core-shell Nanowires Interesting

Nanowires are cylindrical structures characterized by large surface-to-volume ratios and nanoscale cross-sectional areas. One of the primary advantages of NWs is that their radial dimension - lying at or below the length scale of many interesting physical phenomena - can be tuned to optimize or create completely novel optical and optoelectronic effects that could ultimately lead to miniaturized devices with improved properties compared to bulk materials. Fields of applications include energy conversion, electronics, and chemical sensing, among others. Depending on their function, NWs can be made of semiconductors, metals, insulators, and organic compounds.
Semiconducting NWs have shown very promising properties for photovoltaics since by using only a minimal amount of active material they can scatter the light efficiently and can absorb more photons than a comparably thick solid crystalline film [9]. They in fact strongly interact with light via waveguide modes and optical resonances, leading to enhanced optical absorption and photocurrent [10]. Owing to the nanoscale dimensions, the NW geometry offers also the possibility to increase the performance of solar cells when the minority carrier diffusion length drops significantly as in the case of semiconductor materials with a high density of defects. In addition to the above benefits, core-shell semiconducting NWs with radial p-n junctions have shown great potential for improved separation and collection of photogenerated carriers [11]. However, their performance depends heavily on the quality of the junction, which is regulated by the crystallinity of the semiconductor and the doping levels.
Despite the great improvements of the recent years [12-14], combining high charge collection and absorption efficiencies remains an important challenge in semiconducting NWs.
On the other side, NWs made of metal have shown very interesting properties for high-performance transparent electrodes in touch screens, displays and photovoltaics [15]. However, one of the limiting factors for such next generation electrodes is the parasitic optical absorption loss caused by reflected and scattered light [14,16,17]
An ideal situation for the creation of a high-efficiency solar cell would be that of realizing a single device where the optical absorption properties of semiconducting NWs and the electrical properties of highly conductive NWs are combined together.

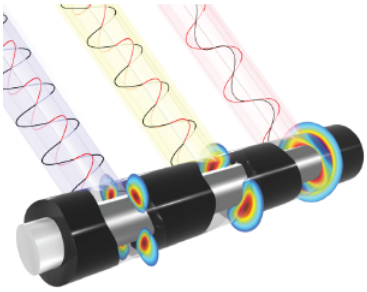

Figure 1.1: Schematic view of a metal-semiconductor core-shell nanowire and its optical resonances [18].

With this goal in mind, the group of Nanoscale Solar Cells at AMOLF - where the present project has been carried out - is investigating a novel NW structure with a metal core embedded

in a thin semiconductor shell (Fig. 1.1). Such geometry would not only have the advantage of reducing significantly the amount of material, but it would also allow to reach high efficiencies regarding both light absorption (that would be even higher than solid semiconducting NWs) and conversion into electricity. In 2013, through theoretical studies on light trapping effects in metal-semiconductor core-shell NWs, Mann & Garnett demonstrated that by ensuring critical coupling one can maximize the absorption of photons exceeding the performance of solid semiconducting NWs [18]. Numerical electromagnetic simulations showed in fact that metal-semiconductor NWs are less sensitive to the polarization of light (Fig. 1.2, green line) compared to solid semiconducting NWs (Fig. 1.2, red line). The highest absorption efficiency would be achieved with NWs with a metal core diameter of ∼100 nm and a semiconductor a-Si shell only 20 nm thick.

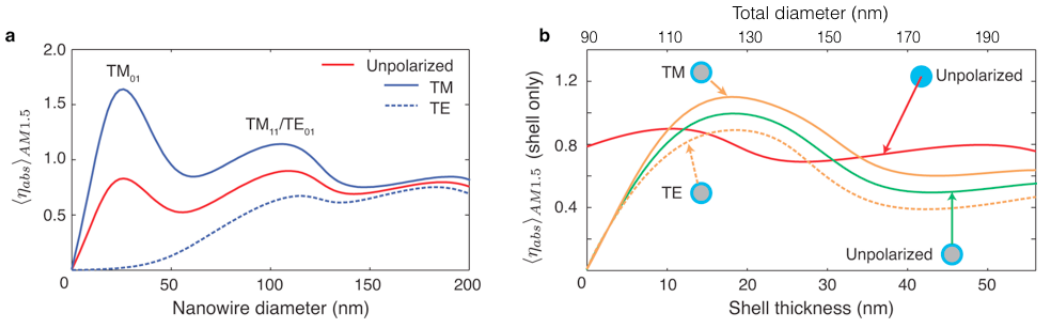

Figure 1.2: Absorption efficiency a) of a solid a-Si nanowire for unpolarized light (red), in TM (blue, solid) and TE (blue, dashed), as a function of diameter, and (b) in a-Si shell wrapped around an 88 nm diameter Ag nanowire as a function of shell thickness for unpolarized light (green), in TM (orange, solid) and in TE (orange, dashed). The red curve is the unpolarized absorption efficiency in a solid a-Si nanowire with the same outer diameter (i.e., from 88 to 200 nm) [18].

Using a simplified explanation, this can be viewed as a result of the fact that not only the plasmonic (Fig. 1.4 a)) and Mie resonances (Fig. 1.4 b)) typical of metal and semiconducting NWs respectively are present, but additional Fabry-Peròt-like resonances are activated by incident light. Thanks to the presence of the metal core photons that have not been absorbed can reflect off each interface of the shell several times, making multiple passes through the semiconductor as in a Fabry-Peròt cavity. This enhances the absorption of TE polarized light in NWs with shell thickness below 20 nm (Fig. 1.2 b), dashed yellow line), which on the other side is weak in the case of small diameter solid semiconducting NWs (Fig. 1.2 a)).

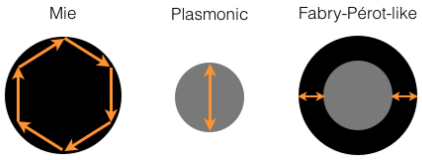

Figure 1.3: Schematic representation of three different types of resonances.

In addition to their outstanding optical properties, metal-semiconductor core-shell NWs can in principle show also a collection efficiency superior to that of solid semiconductor NWs. Although studies have to still verify this hypothesis, the presence of the metal core in semiconductor NWs might be ideal for charge separation and carrier collection.
The theoretically demonstrated enhanced absorption of light and the promising electrical properties make core-shell NWs a very interesting structure to test experimentally, first by carrying studies on individual NWs and then by incorporating them into arrays.
In order to make a photovoltaic device out of single metal-semiconductor core-shell NWs the role of metallic contacts is fundamental, not only to provide a way to extract the photogenerated current, but also for the working principle of the NW solar cells itself. The requirements on the electrical contacts for metal-semiconductor core-shell NW photovoltaics will be presented in the following chapter.

1.3 Aim of this Project

The remarkable performance predicted for core-shell NWs encourages experimental investigation. In order to measure the properties of single NWs one needs to apply electrical contacts to them, one on the core and the other on the shell.
The goal of my project is to provide an efficient and reliable route to fabricate electrical contacts on single metal-semiconductor core-shell NWs using e-beam lithography. In addition, the choice of the metallization scheme plays an important role in determining the performance of the device since the depletion region induced by the metals in the semiconductor serves to separate photogenerated carriers in the opposite directions. My second objective is therefore to find a proper metal that can create a metal-semiconductor junction functional for photovoltaics.

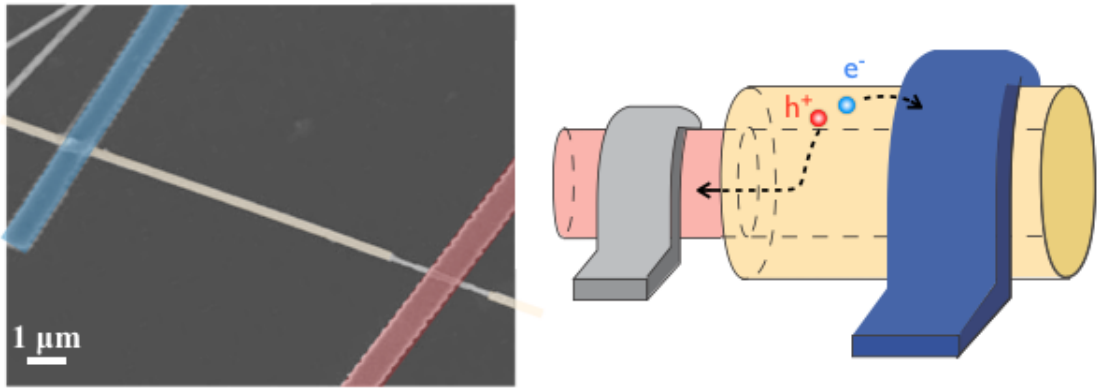

Figure 1.4: On the left, SEM image of core (in red) and shell (in blue) metal contacts on a single NW. On the right, a schematic representation of separation and collection of photogenerated carriers through a contacted NW: the contact in red collects holes, while the one in blue collects electrons.

Chapter 2

Metal Contacts for Photovoltaic Core-Shell Nanowires

A PV device can be created out of core-shell NWs thanks to the junction that is formed between the semiconducting shell and the metal core. The working principle on which it is based is the same as that of a p-n junction, with the difference that instead of achieving the junction through a change in doping, it is achieved through the depletion or inversion layer induced by a metal in contact with the semiconductor.
To work as a solar cell, a single core-shell NW needs to be provided with two metal contacts: one is constituted by the NW core itself, while the other is located on top of the shell (see Fig. 2.1). Another electrode covers a portion of the NW core for extracting the current.

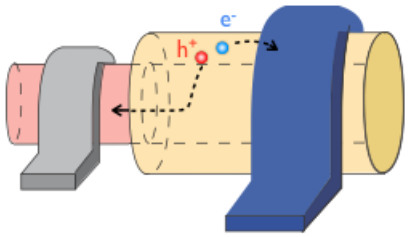

Figure 2.1: Schematic representation of metal contacts on single core-shell NWs for photovoltaics. In this example, the core collects holes (in red) while the shell contact collects electrons (in blue).

The magnitude of the built-in potential field created at the metal-semiconductor interfaces determines the separation of holes and electrons towards opposite sides of the semiconductor, and the collection of them through the respective metal electrodes (in the example in Fig. 2.1, the shell and the core contacts collect electrons and holes respectively). These two processes are fundamental for the performance of a solar cell and a great challenge, in particular for nanoscale-based devices, is to optimize them.
In this section I will briefly review the main processes involved in the operation of solar cells, and I will explain under which criteria metal contacts can be chosen to help separating and collecting the photogenerated charges.

2.1 The Photovoltaic Effect

The photovoltaic effect is the physical process exploited by solar cells to convert the sunlight into electrical current and feed an external load (Fig. 2.2).
The first step in this process consists in the absorption of an incident photon by the active semiconducting layer. By definition, a semiconductor is characterized by a valence band E_V and a conduction band E_C, separated by an energy gap E_{gap}. The energy gap is an intrinsic property of the material, defined as the energy needed to excite an electron from the valence band to the conduction band. When an incident photon has an energy $E_\gamma > E_{gap}$ it gets absorbed by the semiconductor resulting in an electronic excitation in the material.

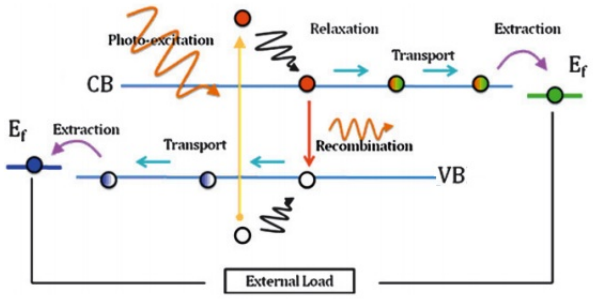

Figure 2.2: Schematic of the physical process involved in PV operation [19].

Once the excited electron and the corresponding hole are separated they form free charges that can be transported through the active layer to the metal contacts. Finally, the carriers have to be extracted. In this way absorbed light is converted into electricity.
However, there are several factors limiting the PV process. Recombination losses (free electrons and holes recombine before reaching the metal contacts) are one of the biggest issues, especially in solar cells based on nanostructures. In fact, due to the very thin active layer and the highly defective quality of the semiconductor, the diffusion length of photogenerated carriers - which is the distance that separated charges can travel before recombining together - is very short. In order to achieve high-efficiency NW solar cells, charge separation and collection have to be improved so that recombination does not dominate. The use of metal electrodes can substantially help in this direction, as I will explain in the following.

2.2 Charge Separation and Collection with Metal Contacts

The separation and collection of charge carriers are processes that compete with the undesirable recombination of excited electrons and holes. In order to optimize them, especially in the case of nanostructures, the designing of the electrodes can play an important role. In particular, the choice of the metallic material is determinant.

In fact, when a metal (or another type of material) is in contact with a semiconductor a built-in potential field is induced at the interface; the magnitude of the potential, given a certain electron affinity and energy gap of the semiconductor, depends on the work function of the metal contact which determines the degree of separation of free carriers in opposite directions. Moreover, based on the difference in work function between the metal and the semiconductor, the electrodes can be specifically designed to selectively collect a specific type of carrier (i.e., either electrons or holes).
From an electronic band structure standpoint, when the materials are put into contact, the energy bands of the semiconducting layer align with the Fermi energies E_F of the other material to restore the equilibrium in the system. The resulting band bending of the energy levels dictates the flow of carriers across the hetero-junction and through the metal contacts. The efficiency of both processes - charge separation and collection - can therefore be optimized by properly choosing the metallization scheme.
Figure 2.3 shows a schematic representation of the energy band diagram of an ideal configuration for a metal-semiconductor-metal system.

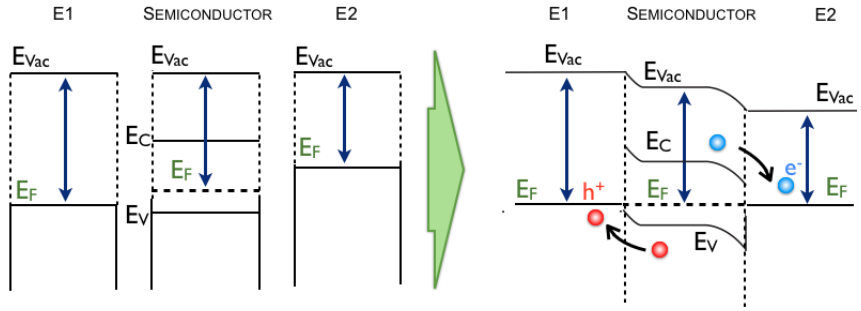

Figure 2.3: Energy band diagrams of the semiconductor and of the two electrodes $E1$ and $E2$ with higher and lower work function than that of the semiconductor respectively, when separated (on the left) and when in contact (on the right).

On the left of Fig. 2.3 the three materials are isolated and each of them is characterized by a higher or lower density of electrons, related to their work function ϕ. The work functions are chosen in a way that they satisfy:

$$\phi_{E1} > \phi_S > \phi_{E2}$$

When the materials are brought into contact the energy of the system has to redistribute, so the electrons flow from the semiconductor to the electrode with higher work function ($E1$), and from the electrode with lower work function ($E1$) to the semiconductor.
In this way, the semiconductor is depleted of electrons in the region adjacent to $E1$ which becomes negatively charged, while is depleted of holes in the region in contact with $E2$, that becomes positively charged. This results in the formation of a space-charge region similar to a p-n junction, essential for the PV operation in metal-semiconductor core-shell NWs.
For my project I used NWs made of either Ag or Au for the metal cores, and of Cu_2O for the semiconducting shell. They have been provided to me by Beniamino Sciacca - a post-doc in our group of Nanoscale Solar Cells - and they have been synthesized in solution. To create the metal NWs he followed the procedure reported by Sun et al. [20], and he used the one by Kuo

et al. to then grow the Cu_2O shell around them [21].
Fig. 2.4 a) is a scanning-electron-microscopy (SEM) image of the cross section of a Ag@Cu_2O NW, while b) and c) are tunneling-electron-microscopy (TEM) images of the atomic structure of the Cu_2O shell grown on Ag and Au NWs respectively. The atoms of the shell clearly follow the crystal orientation of the metal seed. Therefore the nature of the Cu_2O material is crystalline. This fact represent an important advantage for the solar cell performance from an electrical standpoint.
The doping of Cu_2O depends on the synthesis method that has been employed, but the material is usually found to be a p-type semiconductor. It has a direct energy gap $E_g \sim 2$ eV that could theoretically allow to achieve solar cell efficiencies around 20%. Its work function is around 4.8 eV.

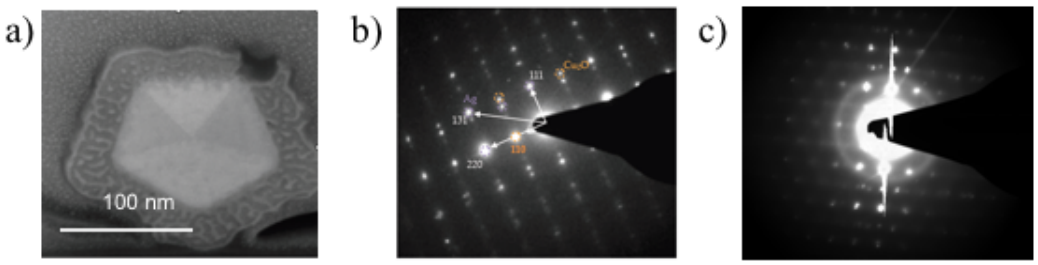

Figure 2.4: a) A SEM image of a NW cross section shows the pentagonal shape of the Ag NW core and the Cu_2O shell uniformly covering the metal seed.
b) and c) are TEM images representing the diffraction of the Cu_2O layer grown on top of Ag and Au respectively. In both cases the crystalline orientation of Cu_2O follows that of the metal core and the nature of the material is crystalline. Note: the above results have been acquired by Beniamino Sciacca.

Chapter 3

Design and Fabrication

Here I describe the fabrication process that I developed to create electrical contacts to individual core-shell nanowires.
In general, the main fabrication steps are: the substrate preparation, the nanowire dispersion, the patterning with electron-beam lithography, the metallization and the lift-off.
The procedure is repeated twice to fabricate the core and the shell contacts. They need to be separate processes, first, because for the core contacts an additional step prior the metal deposition is needed to etch away the semiconducting shell underneath the contact area; secondly, the type of deposited metals is different.
For my experiments I used 4×4 mm^2 Si/Si_3N_4 chips as device substrates, provided with Au pads and alignment markers previously patterned by photo-lithography (Fig. 3.1 a)). The silicon nitride layer of about 300 nm provides good electrical insulation preventing current leakage from the metal contacts to the silicon wafer. Moreover, for future optical absorption measurements, a window in the Si substrate can be opened so that only the Si_3N_4 membrane is left, providing a mechanical support for the NWs that is transparent to light.
The nanowires are transferred on each sample using a wet dispersion method. A drop of solution containing NWs dispersed in a mix of ethanol and water is added on the chip, letting the solvent to almost or completely evaporate. The chip is then cleaned by dipping it first in acetone and subsequently in ethanol, to remove any left residue.
By inspecting the sample with an optical microscope after each drop casting one can control the density of deposited nanowires, that scatter the light and are therefore easily recognizable. If the density is too low the drop casting is repeated. The squared field of view (FOV) determined by the rectangular ends of the Au pads (Fig. 3.1 b)) constitutes the working field for my experiments and its dimensions are 300×300 μm^2.

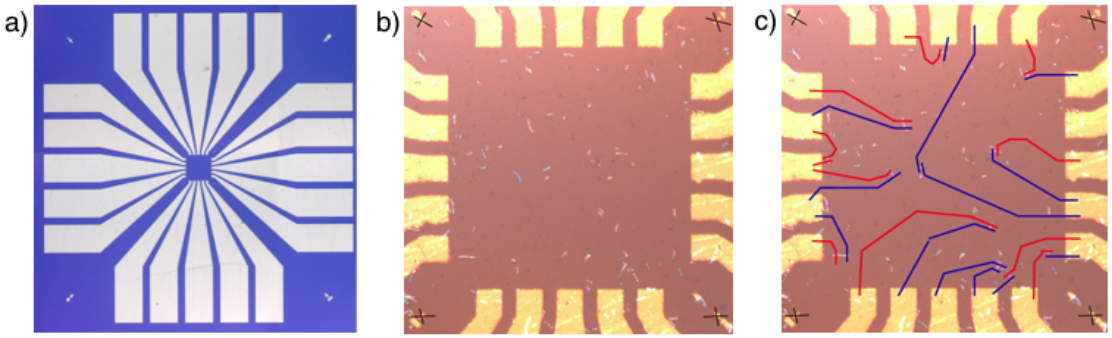

Figure 3.1: a) Optical microscope image of the 4 × 4 mm^2 chip used for fabrication: the substrate appearing in blue is made of Si, covered by a thin Si_3N_4 membrane. The features coloured in white correspond to the gold pads, with markers on each corner.
b) Optical microscope image of the central area of the chip (FOV) with dropcasted NWs scattering the light.
c) Drawings on the same FOV shown in b) of black cross markers and red and blue lines representing the core and shell contacts to single NWs respectively.

Once the drop-casting procedure is finished, an image is acquired, registering the position of the NWs in the FOV (Fig. 3.1 b)). The image is used to draw core and shell contacts on single NWs using an appropriate graphic software (e.g., Adobe Illustrator) (Fig. 3.1 c)). Crosses are drawn to identify the position of the markers.
The drawings relative to one type of contacts (i.e., red or blue lines) are then exported, together with the cross marks, into a CAD file. Using an e-line software a width is assigned to the contacts (0.5 μm and 1 μm for the core and shell contacts respectively), the distance between the markers is scaled to adjust it to the actual designed distance (200 μm), and 3 markers are added in proximity of the crosses. The markers are used to correct for misalignments by manually finding them through a quick scan of the sample, prior the patterning of the contacts with the electron beam.
Once the files are ready, the sample can be prepared for patterning the contacts with e-beam lithography.
The fabrication is described in detail in the following sections.

3.1 Fabrication Process using E-beam Lithography

Since the NWs are randomly distributed in the FOV, the pattern of the contacts that has to be written is different from sample to sample. For this reason, e-beam lithography is the most convenient technique among others (e.g., photo-lithography) for writing the contact electrodes on single NWs.
I used a Raith 150 electron-beam lithography system, capable to control and place patterns with a resolution better than 50 nm, making it well suited for contacting nanowires. The e-line system uses a hardware like a scanning electron microscope (SEM).

The step-by-step process of fabricating metal contacts on NWs by electron beam lithography

is shown in Fig. 3.2. The recipe is reported in detail in *Appendix*.

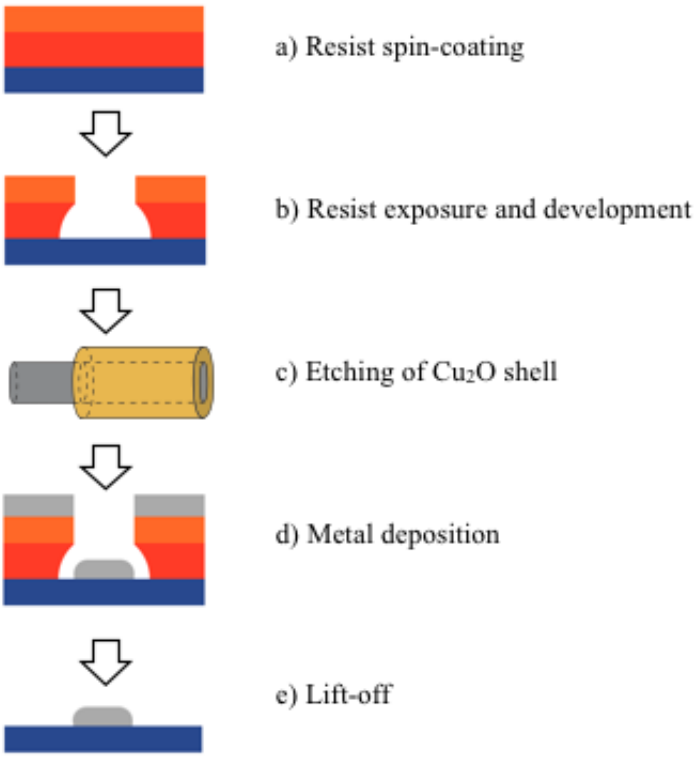

Figure 3.2: Schematic representation of the fabrication process

To start with, the sample is coated with a layer of positive resist for e-beam lithography - an electron-sensitive polymer, that becomes soluble in an appropriate developer solution after exposure (Fig. 3.2 a)).
For my purposes I used a bi-layer recipe: the resist for the bottom layer (MMA 9% in Ethyl Lactate) is chosen such that it develop faster than the one for the top layer (PMMA 11% in Anisole). This allows to create the undercut schematically shown in Fig. 3.2 b), which makes easier the lift-off of deposited metals later on (Fig. 3.2 e)).
Another requirement for a successful lift-off is that the thickness of the resist bi-layer has to be at least twice the thickness of the deposited metal (in my case, up to 300 nm).
I therefore ran a test experiment where I optimized the spin-coating parameters (spinning rate, time and acceleration) in order to get a uniform layer thickness of $\sim$ 800 nm. The uniformity of the layer is important to avoid problems relative to the dose used for the e-beam exposure. The dose in fact depends on the thickness of the resist - among other variables - so if the layer is not equally distributed all over the sample some regions might be over- or under-exposed, eventually leading to imperfections (e.g., cracks) in the metals contacts. An example of a consequent problem of under-exposure encountered along the way is shown in Fig. 3.3. The parallel cracks seem to correspond to the edges of the rectangular shape of the spot size of the e-beam, where in fact the dose is always lower compared to the center of the spot. Therefore,

the edges do not receive enough dose to be removed by the developer solution.

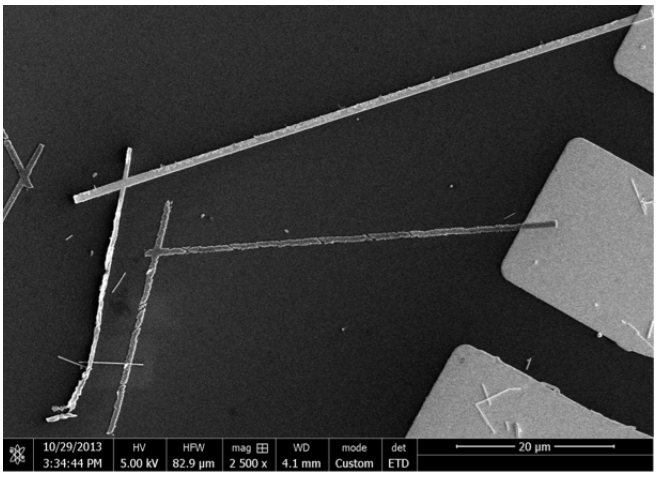

Figure 3.3: SEM image representing an example of a dose problem: the under-exposure causes that the resist is not developed uniformly, which results in cracks along the contacts after the metal deposition.

After each spinning, the sample is baked on a hot plate to harden the resist layer.
Once the spin-coating recipe has been improved, the dose has to be accurately calibrated before performing the lithography for single-NW device fabrication. To determine the optimal exposure parameters I used a method based on dose modulation. The method consists in writing a grid of identical patterns and progressively increasing the dose in each of them. The patterns are based on lines of different size, imitating the NW electrical contacts. The dose for the first pattern is set below the expected optimal value and the step by which the dose is increased for subsequent lines is chosen small enough to determine the optimal value. Microscopy inspections after metallization and lift-off allow then to choose the optimal dose.
Ultimated the dose test the following step consists in patterning the electrodes by electron beam. I used a MIBK:IPA 1:2 as developer solution for 1 minute and 30 seconds (Fig. 3.2 b)). Once the windows have been opened the following step for the shell contacts is to deposit the metal layer (Fig. 3.2 d)).
In the case of the core contacts an additional step prior the metallization is required to remove the underneath semiconducting shell (Fig. 3.2 c)). This is achieved by dipping the sample in a solution of 0.1 mM sulphuric acid (H_2SO_4) for approximately 3 minutes, and then immediately rinsing it in water to stop the reaction.
After the metal deposition, the remaining resist is dissolved in acetone and only the metal contact pattern stays after the lift-off (Fig. 3.2 e)).

3.2 Metallization Schemes

The metallization is the fabrication step in which electrical contacts are formed by depositing selected metals. There are several methods of metallization, such as thermal evaporation and DC sputtering (Fig. 3.4 a) and b), respectively). The main difference between these two techniques is that with thermal evaporation the deposition is directional, while with sputtering a conformal coverage is obtained.

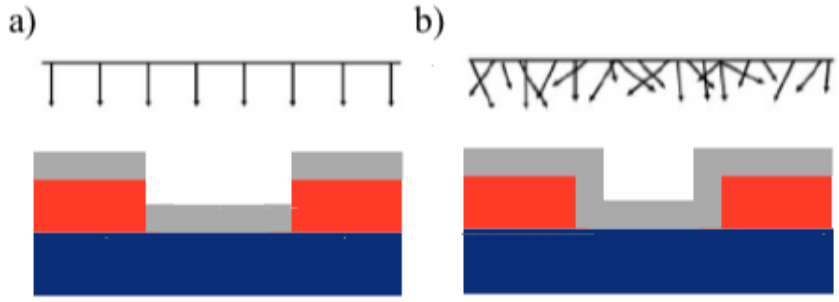

Figure 3.4: Schematic representation of two metal deposition methods: a) thermal evaporation and b) DC sputtering. The black arrows indicate the direction of the flow of metal particles.

Given that the NWs have average diameters around 150 nm, in order to avoid discontinuities in the metal contacts, the layer thickness should be at least 250 nm if deposited by thermal evaporation, while only 80 nm if deposited by sputtering. Although the sputtering technique provides the advantage of wasting less material, the lift-off of sputtered metal of such a thickness is usually made difficult by the conformal coating of the resist walls (see Fig.3.4 b)), that might not allow the developer solution to penetrate everywhere and remove the metal from unwanted regions. On the other side, even 250 nm of material deposited by thermal evaporation can be easily lifted away.
For this reason, at the beginning of my project I used only thermal evaporation to fabricate the contacts.
Interestingly, later on I ran an experiment to test wether also a sputtering method could be employed, and I found out that my resist recipe was suitable for the lift-off of metal layers deposited via this technique as well. That resulted in the advantage of speeding up significantly the fabrication process, besides wasting less material. Sputtering in fact requires only few minutes, while thermal evaporation requires up to 10 hours due to the high quality vacuum that needs to be created inside the chamber prior deposition and the slightly slower deposition rate of the process itself.
However, it is not always convenient to deposit metals of at least 80 nm using a DC sputtering method. In fact, the deposition of layers of such a thickness, if the metals are easily oxidizable by nature (as in the case of aluminium and titanium) can take up to several hours.
An overview on the metallization schemes that I tested in my experiments is given in Table 3.1. The choice of the materials for the core and the shell contacts has been performed on the basis of the values of their work functions found on the web in comparison to those of the NW materials, following the considerations given in Section 2.2.

The deposition method used to fabricate the contacts is included in Tab. 3.1 as well.
The results of the measurements that I obtained using these metallization schemes will be discussed in the next chapter.

Ag@Cu_2O NWs			
Au $\rightarrow \phi$ 5.1 eV		$Cu_2O \rightarrow \phi$ 4.6 - 4.8 eV	
Metallization schemes			
Core		**Shell**	
Deposited material	ϕ **[eV]**	**Deposited material**	ϕ **[eV]**
sputtered Au	5.1	sputtered Au	5.1
sputtered Ag	4.7	sputtered Au	5.1
sputtered Ag	4.7	evaporated Al	4.2

Au@Cu_2O NWs			
Ag $\rightarrow \phi$ 4.7 eV		$Cu_2O \rightarrow \phi$ 4.6 - 4.8 eV	
Metallization schemes			
Core		**Shell**	
Deposited material	ϕ **[eV]**	**Deposited material**	ϕ **[eV]**
sputtered Au	5.1	evaporated Ti	3.9

Table 3.1: Tested metallization schemes for the different NW materials: Ag@Cu_2O (top table) and Au@Cu_2O (bottom table). The work function ϕ and the chosen deposition method for each type of metal are also indicated.

Chapter 4

Results and Discussion

As a first step I wanted to explore the properties of Cu_2O and in particular wether the difference in work function between the semiconductor and the metal core allows the passage of majority carriers across the contact interface. From now on we will assume that the semiconductor is p-doped, thus the majority and minority carriers are holes and electrons respectively.
In the case of Ag@Cu_2O NWs, Ag has a work function around 4.6 eV, but the one of Cu_2O can vary from 4.7 to 4.9 eV depending on the synthesis method [22,24]. If the two work functions are similar, holes can flow through the metal contact; otherwise, they see a barrier and they are rectified. I therefore wanted to verify this, by using an appropriate metallization scheme.

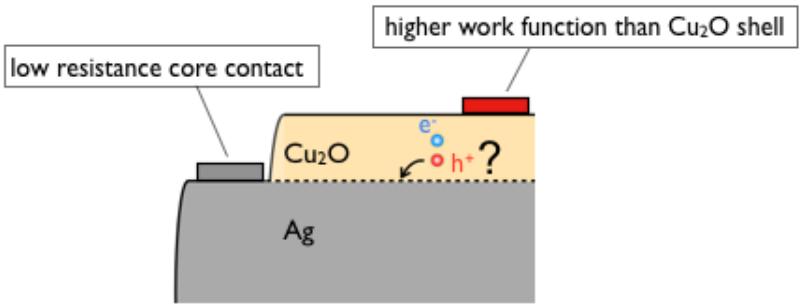

Figure 4.1: Schematic representation of the metal contacts on single-Ag@Cu_2O NWs required to test wether the difference in work function between Cu_2O and Ag is small enough to allow holes to pass across the metal-semiconductor interface.

For my purposes I needed a metallization scheme where the metal contact for the shell had a work function certainly higher than that of the semiconductor; no particular requirements were present instead for the metal of the core contact, although an advantage would have been that of having as low resistance as possible (Fig. 4.1).
Gold seemed to be a metal with optimal properties for both the core and the shell contact, given its high work function and conductivity.
However, SEM images acquired after fabrication revealed that the presence of Au particles on

the Ag NW core induced a degradation of the NW itself (Fig. 4.2, on the left). On the other hand, no degradation was occurring when the Au contacts were laying on the semiconductor (Fig. 4.2, on the right). An article published by Grouchko et al. clarified the origin of this problem, suggesting it was due to a diffusion mechanism caused by differences in activation energies between Au and Ag [23].

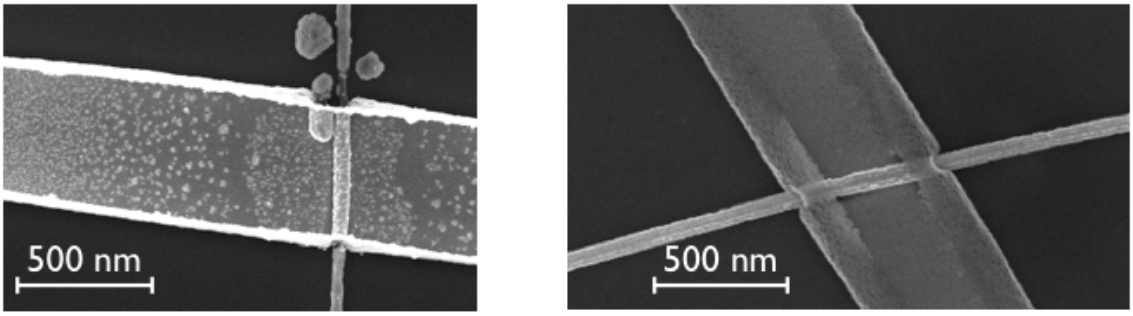

Figure 4.2: SEM images of a NW degraded by the sputtered Au contact on the core (on the left) and of a NW not degraded by the sputtered Au contact on the shell (on the right).

I therefore tried another metallization scheme for the Ag@Cu_2O NWs, employing Ag and Au as core and shell contacts, respectively. This time no degradation problems were encountered and I could measure the current-voltage characteristics of individual NWs.
For my measurements I used an Agilent software (model B1500A) connected to a micromanipulator probe station. By placing the needles of the micromanipulator on top of the chip gold pads relative to the pair of electrical contacts of the NW I wanted to measure, I could apply a bias voltage and measure the current.
Fig. 4.3 shows the I-V curves of a single Ag@Cu_2O NW recorded in the dark (in black) and under 1 sun illumination (in orange).
The current increases in good approximation linearly with the bias voltage suggesting that the work function of the Ag core is not significantly smaller than that of the Cu_2O shell, thus allowing the majority carriers to easily overcome the potential barrier at the interface and be collected by the Ag electrical contact.
Moreover, a photoconductivity effect has been detected: upon the absorption of light the number of free carriers in the semiconductor increased leading to a higher current compared to the that extracted in the dark from the same NW. Under 1 sun illumination, at the highest applied voltage of 1V a current of $\sim$ 50nA has been measured, 10 nA higher than in the dark. The presence of photoconductivity encouraged to further proceed with the experiments.
Knowing that the majority carriers were easily collected by the metal core I could start thinking of a material that could substitute the Au for the shell contact in order to realize a metallization scheme functional for photovoltaics.

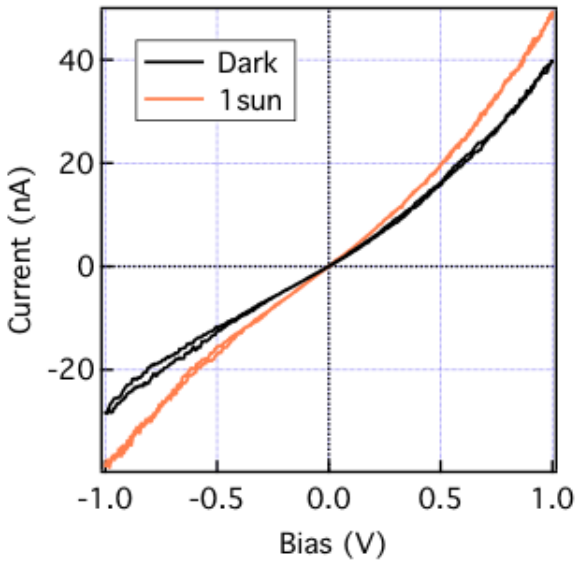

Figure 4.3: I-V curve in the dark (black) and under 1 sun illumination (orange) of a single Ag@Cu_2O NW with Ag and Au electrical contacts for the core and the shell respectively.

In order to create solar cells out of single Ag@Cu_2O NWs I had to find a material for the shell contacts having a work function lower than that of Cu_2O, such that the barrier created at the metal-semiconductor interface would have rectified majority carriers while collecting the minority ones. On the basis of the values available in the literature [22], titanium and aluminium appeared to be two metals that could have potentially served the function well (Tab. 3.1, Chap. 3).

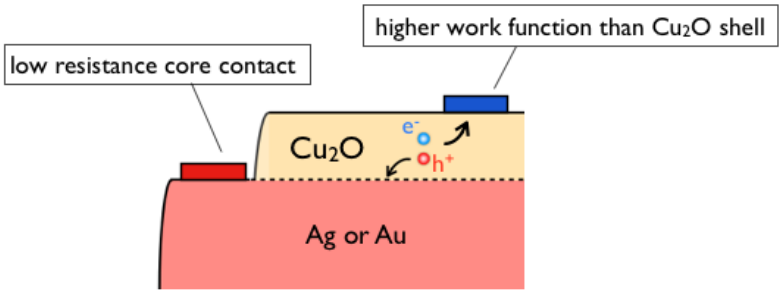

Figure 4.4: Schematic representation of a cross section of the metal contacts on single metal-semiconductor NWs (with Ag or Au as materials for the core, and Cu_2O as semiconductor) with the requirements for creating a photovoltaic device. The shell should be designed in a way that it collects the minority carriers, i.e. electrons.

I started by fabricating electrical contacts to Ag@Cu_2O NWs using Ag for the core contact and Al for the shell contact. The measurements, however, lead to no successful result. This was due to the fact that, as reported in the literature, aluminium forms an intra-metallic layer with gold that does not conduct [25]. For this reason, being the electrical pads of the chip

made of Au, Al had to be excluded as metal candidate for the NW contacts.
I then decided to use Ti instead. In the mean time, I found out that the Ag@Cu_2O NWs of the solution I was using were degrading very fast after the drop-casting. I therefore switched to Au@Cu_2O NWs, which turned out to be chemically more stable.
Current-voltage measurements performed on Au@Cu_2O NWs with Ti shell contacts and Au core contacts gave very interesting results (Fig. 4.5). First of all, a strong rectifying behavior and an increase in conductivity from dark to 1sun-illumination measurements have been detected. The current rectification for negative values of bias voltage indicates that the potential barrier created between Ti and Cu_2O is large enough for not allowing majority carriers to penetrate through the interface.

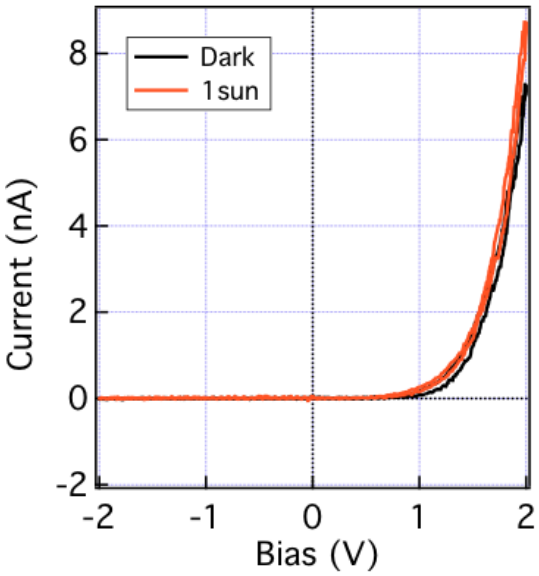

Figure 4.5: IV curves in the dark (black) and under 1 sun illumination (orange) of Au@Cu_2O NWs contacted with Ti on the shell and Au on the core.

However no photocurrent (i.e., current at zero bias) has been measured at 1 sun illumination. This result suggests that the number of photogenerated minority carriers is too low to contribute to an appreciable current and that their diffusion length is too short to allow to those generated far away from the electron-collector electrode to reach the metal without recombining.
The contacted Au@Cu_2O NWs therefore behave as very efficient diodes, but not yet as photovoltaic devices.
To gain more insight on the properties of Au@Cu_2O NWs, their I-V characteristics were measured again, while the NWs were locally illuminated at different positions by a 200 μW laser diode (λ= 404 nm).

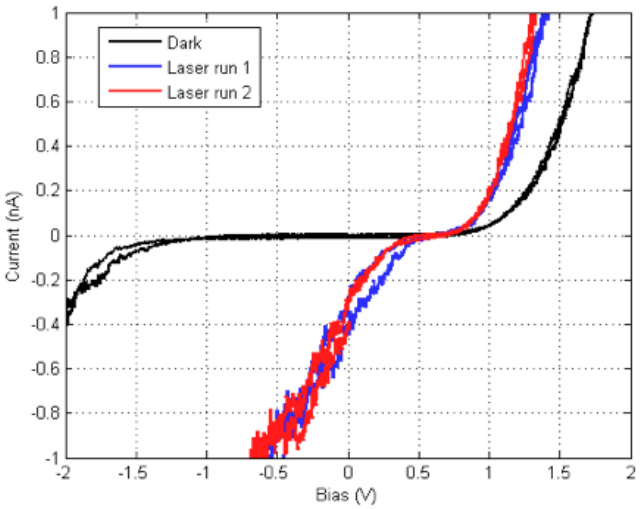

Figure 4.6: IV curves in the dark (black) and under 1 sun illumination (orange) of Au@Cu_2O NWs contacted with Ti on the shell and Au on the core.

By focusing the laser in proximity of the shell contact we were able to measure a photocurrent of $\sim$ 400 pA (Fig. 4.6).
This result is in line with what was found before: under 1 sun illumination the density of minority carriers is too low, but increasing the power of illumination and focusing it in proximity of the area where the presence of a space-charge region is expected, a photocurrent can be detected.
Metal-semiconductor core-shell NWs demonstrated therefore both photoconductivity and photocurrent, although improvements have to be performed to create a device useful for real photovoltaic applications.

Chapter 5

Conclusions and Future Prospects

With the present report I investigated the properties of single core-shell NWs with Cu_2O as semiconducting shell and Ag or Au as metal cores.
I created an efficient and reliable technique for fabricating electrical contacts to them and I tested different metallization schemes that could lead to a photovoltaic device.
Measurements on single Ag@Cu_2O NWs with Ag core and Au shell contacts showed that the work function of the Cu_2O semiconductor must be similar to that of Ag (4.6 eV), since the increase of current with applied voltage is almost linear. Moreover, a photoconductivity effect has been detected, giving a 10 nA increase in current at 1V, passing from dark to 1 sun illumination measurements.
Degradation problems on Ag@Cu_2O NWs encountered along the experiments forced to switch to Au@Cu_2O NWs.
With these NWs I tested another metallization scheme, potentially functional for photovoltaics: I employed Ti as shell contact and Au as core contact.
The I-V characteristics of such single-NW devices showed again photoconductivity effects, and in particular a strong rectifying behavior.
However, no photocurrent has been measured at 1 sun illumination, suggesting that the density of minority carriers is too low and that the diffusion length is too short.
Increasing the power of illumination using a 200 μW 404 nm diode laser, focused in proximity of the shell contact of a single NW, allowed to measure a photocurrent of $\sim$400 pA.
In conclusion my experiments have proven the efficacy of the method for contacting metal-semiconductor core-shell NWs giving an insight on their properties, with encouraging results.
In order to make a photovoltaic device operative at 1 sun illumination and with higher efficiency more efforts are still required.
A possible improvement that could be immediately tested consists in depositing a thin Ti layer (approximately 5 nm thick) along the NW shell in a way that the electron-collector electrode extends throughout the structure, collecting the minority carriers generated also far away from the contact area. Future experiments will be carried out to try out this test.

Appendix A

Details of the Fabrication Process

NW drop-casting

- Drop-casting of $\sim 10\mu$L of NWs dispersed in a solution of Ethanol and water;

- Spontaneous drying of NW solution;

- Rinsing of the sample in Acetone ($\sim$ 30 s) and consecutively in IPA ($\sim$ 30 s).

Spin-coating of Resist Bi-layer with a *Suss Delta 80* system

- **Layer 1**: MMA 9% in Ethyl-Lactate

→ spin-coating @ 2000 rpm and 3900 rpm/s (expected thickness = 500 nm);
→ pre-baking 1' @ 150°C on hotplate;

- **Layer 2**: PMMA 950k 4% in Anisole

→ spin-coating @ 4000 rpm and 3900 rpm/s (expected thickness = 400 nm);
→ pre-baking 1' @ 180°C on hotplate;

Exposure with a *Raith e-LiNE* e-beam lithography system

Beam energy = 20 kV ; Aperture = 10 μm; Dose = 350 μC/cm^2.

Resist Development

- Development in MIBK:IPA = 1:2 for 90 s;

- Rinsing in IPA.

Shell Etching (only for Core Contacts)

- Etching in H_2SO_4 0.1 mM for 3';

- Rinsing in water for 1'.

Metal deposition

- Thermal evaporation of metals (Al, Ti) with *Kameleon*, an e-beam PVD system

Deposition rate:

→ 0.5 $\mathring{A}$/s for the first 50 nm;
→ 1.3 - 1.7 $\mathring{A}$/s for reaching the desired final thickness ($\sim$ 300 nm)

- DC Sputtering of metals (Au, Ag) with a *Emitech 575DX* system

Desired final thickness: 80-90 nm.

Lift-off

- Lift-off in warm Acetone (45°C) for 1 hour;

- Rinsing in IPA.

Aknowledgements

Performing my internship project in the Nanoscale Solar Cells group has been a wonderful and rewarding experience. I worked with great enthusiasm for the improvement of the core-shell NW technology and I wish to thank all the people who helped me accomplishing my goals and who allowed me to spend beautiful six months inside AMOLF.
In particular, I want to express all my gratitude to Erik, my group leader, for supervising my work and keeping my motivation always high thanks to his scientific competence, positivity and enthusiasm. His scientific and communicational approach will constitute for me a model to follow in my future career. With this respect, I would like to thank also the second supervisor of my internship project, Gao, for his great disponibility and support.
It is important for me to underline that my project would have never been possible without the contribution of other members of AMOLF. I especially value very much the support of the Nanoscale Solar Cells group, including Sebastian, Beniamino, Sander, Mohammed, Parisa, Micheal, Gede, Jantina, Jia e Sarah. In particular, Sebastian has been a great mentor, teaching me how to handle and manipulate the tiniest devices. Beniamino has constantly supplied me with his magic solutions of core-shell NWs, without which I would have not gone too far. Sander has been fundamental to motivate all my efforts and hours in the lab thanks to his advanced theoretical studies. A special thanks also to Parisa, for the idea of brightening our shared office with colourful flowers.
In addition, I want to thank the technicians Andries, Dimitry and Hans for their indespensable support during my fabrication processes.
Last but not least, my internship project gave me the opportunity to meet wonderful people, who I thank for the great time they made me spend. Among these, stand out my current housemates, Lutz and Jeanette - also members of AMOLF - who are among the most inspirational people I have ever met. Moreover, with their generosity and friendliness they made me feel very much at home even in a city, Amsterdam, that is not my hometown.
In conclusion, I thank my family for the most genuine love they provide me with. I thank my father Antonio, for the unfailing support and encouragement, and for being the one who introduced me to the world of nanotechnology, which is today my passion and my work; my sister Francesca, for being my guide in life.
I dedicate this project, conclusion of my enriching and challenging career as a Master student of Applied Physics, to my beloved mother Angela.

Bibliography

[1] P. Frankl, *Technology Roadmap Solar Photovoltaic energy*, Technical report, International Energy Agency, 2010.

[2] N. Lewis, D. Nocera, *Powering the planet: Chemical challenges in solar energy utilization*, Proceedings of the National Academy of Science **103**, 15729-15736 (2006).

[3] M. Green, *Third Generation Photovoltaics: Ultra-high Conversion Efficiency at Low Cost*, Progress in Photovoltaics: Research and Applications **9**, 123 (2001).

[4] E. Garnett, P. Yang, *Light Trapping in Silicon Nanowire Solar Cells*, Nano Letters **10**, 1082-7 (2010).

[5] M. M. Adachi, M. P. Anantram, K. S. Karim, *Core-shell silicon nanowire solar cells*, Scientific Report **3**, 1546 (2013).

[6] B. M. Kayes, H. A. Atwater, N. S. Lewis, *Comparison of the device physics principles of planar and radial p-n junction nanorod solar cells*, Journal of Applied Physics **97**, 114302 (2005).

[7] H. He, C. Liu, K. D. Dubois, T. Jin, M. E. Louis, G. Li, *Enhanced Charge Separation in Nanostructured TiO_2 Materials for Photocatalytic and Photovoltaic Applications*, Industrial & Engineering Chemistry Research **51**, 11841-11849 (2012).

[8] M. Kelzenberg, S. Boettcher, J. Petykiewicz, D. Turner-Evans, M. Putnam, E. Warren, J. Spurgeon, R. Briggs, N. Lewis, and H. Atwater, *Enhanced absorption and carrier collection in Si wire arrays for photovoltaic applications*, Nature Materials **9**, 239 (2010).

[9] F. A. Ponce, D. P. Bour, *Nitride-based semiconductors for blue and green light-emitting devices*, Nature **386**, 351 (1997).

[10] E. Garnett, M. L. Brongersma, Y. Cui, M. D. McGehee, *Nanowire Solar Cells*, Annual Review of Materials Research **41**, 269 (2011).

[11] B. M. Kayes, H. A. Atwater, N. S. Lewis, *Comparison of the device physics principles of planar and radial p-n junction nanorod solar cells*, Journal of Applied Physics **97**, 114302

(2005).

[12] J. Tang, Z. Huo, S. Brittman; H. Gao, P. Yang, *Solution processed core-shell nanowires for efficient photovoltaic cells*, Nature Nanotechnology **6**, 568-72 (2011).

[13] T. J. Kempa, J. F. Cahoon, S.-K. Kim, R. W. Day, D. C. Bell, H. G. Park, C. M. Lieber, *Coaxial Multishell Nanowires with High-Quality Electronic Interfaces and Tunable Optical Cavities for Ultrathin Photovoltaics*, Proceeding of the National Academy of Sciences **109**, 1407 (2012).

[14] J. Wallentin, N. Anttu, D. Asoli, M. Huffman, I. Aberg, M. H. Magnusson, G. Siefer,P. Fuss-Kailuweit, F. Dimroth, B. Witzigmann, H. Q. Xu, L. Samuelson, K. Deppert, M. T. Borgstrom, *InP nanowire array solar cells achieving 13.8% efficiency by exceeding the ray optics limit*, Science **339**, 1057-1060 (2013).

[15] D. S. Hecht, L. Hu, G. Irvin, *Emerging transparent electrodes based on thin films of carbon nanotubes, graphene, and metallic nanostructures.* Advanced Materials **23**, 1482-513 (2011).

[16] J. Y. Lee, S. T. Connor, Y. Cui, P. Peumans, P. *Solution-Processed Metal Nanowire Mesh Transparent Electrodes* Nano Letters **8**, 689-692 (2008).

[17] J. Van de Groep, P. Spinelli, A. Polman, *Transparent conducting silver nanowire networks.* Nano Letters **12**, 3138-3144 (2012).

[18] S. A. Mann and E. Garnett, *Extreme Light Absorption in Thin Semiconductor Films Wrapped around Metal Nanowires.* Nano Letters **13**, 3173-3178 (2013).

[19] Y. Kanai, Z. Wu, J. C. Grossman, *Charge separation in nanoscale photovoltaic materials: recent insights from first-principles electronic structure theory*, Journal of Materials Chemistry **20**, 1053-1061(2010).

[20] Y. Sun, B. Gates, B. Mayers, and Y. Xia, *Crystalline Silver Nanowires by Soft Solution Processing*, Nano Letters **2**, 165-168 (2012).

[21] C.-H. Kuo, T.-E. Hua, M. H. Huang, *Au Nanocrystal-Directed Growth of Au-Cu_2O Core-Shell Heterostructures with Precise Morphological Control*, Journal of American Chemical Society **131**, 17871-17878(2009).

[22] W.-Y. Yang, S.-W. Rhee *Effect of electrode material on the resistance switching of Cu2O film*, Applied Physics Letters **91**, 232907 (2007).

[23] M. Grouchko, P. Roitman, X. Zhu, I. Popov, A. Kamyshny, H. Su, S. Magdassi *Merging of metal nanoparticles driven by selective wettability of silver nanostructures*, Nature Communication **5**, 3994 (2014).

[24] J. A. Assimos, D. Trivich *The photoelectric threshold, work function, and surface barrier potential of single-crystal Cuprous Oxide*, Physica Status Solidi A **26**, p. 477 (1974).

[25] J. A. Jones *Gold aluminium intermetallics current and future considerations*, Electronic Component Conference, European Space Agency, p. 477 (1997).